Atmos. Chem. Phys. Discuss., doi:10.5194/acp-2016-365, 2016
Manuscript under review for journal Atmos. Chem. Phys.
Published: 9 June 2016

Atmospheric Chemistry and Physics Discussions

On-line single particle analysis of ice particle residuals from mountain-top mixed-phase clouds using laboratory derived particle type assignment

S. Schmidt[1], J. Schneider[1], T. Klimach[1], S. Mertes[2], L.P. Schenk[2], J. Curtius[3], and S. Borrmann[1,4]

[1]Particle Chemistry Department, Max Planck Institute for Chemistry, 55128 Mainz, Germany
[2]Leibniz Institute for Tropospheric Research, 04318 Leipzig, Germany
[3]Institute for Atmospheric and Environmental Sciences, Goethe-University of Frankfurt am Main, 60438 Frankfurt, Germany
[4]Institute for Atmospheric Physics, Johannes Gutenberg University, 55128 Mainz, Germany

Correspondence to: J. Schneider (johannes.schneider@mpic.de)

Abstract. In-situ single particle analysis of ice particle residuals (IPR) and out-of-cloud aerosol particles was conducted by means of laser ablation mass spectrometry during the intensive INUIT-JFJ/CLACE campaign at the high alpine research station Jungfraujoch (3580 m a.s.l.) in January/February 2013. During the four week campaign more than 70000 out-of-cloud aerosol particles and 595 IPR were analyzed covering a particle size diameter range from 100 nm to 3 µm. The IPR were sampled during 273 hours while the station was covered by mixed-phase clouds at ambient temperatures between -27 °C and -6 °C. The identification of particle types is based on laboratory studies of different types of biological, mineral and anthropogenic aerosol particles. As outcome instrument specific marker peaks for the different investigated particle types were obtained and applied to the field data. The results show that the sampled IPR contain a larger relative amount of natural, primary aerosol, like soil dust (13 %) and minerals (11 %), in comparison to out-of-cloud aerosol particles (2 % and <1 %, respectively). Additionally, anthropogenic aerosol particles, like particles from industrial emissions and lead-containing particles, were found to be more abundant in the IPR than in the out-of-cloud aerosol. The out-of-cloud aerosol contained a large fraction of aged particles (30 %, including organic material and secondary inorganics), whereas this particle type was much less abundant (3 %) in the IPR. In a selected subset of the data where a direct comparison between out-of-cloud aerosol particles and IPR in air masses with similar origin was possible, a pronounced enhancement of biological particles was found in the IPR.

1 Introduction

Depending on their chemical and microphysical properties aerosol particles have a strong impact on the solar radiation budget, an influence on the life-time of clouds and hence also on precipitation (direct and indirect effect; Lohmann and Feichter, 2005). In the mid-latitudes the formation of precipitation occurs mainly via the ice phase. Ice formation can be initiated in the atmosphere either homogeneously or heterogeneously. Spontaneous freezing of cloud droplets at temperatures lower than -37 °C without any catalysts is called homogeneous freezing (Cantrell and Heymsfield, 2005). At temperatures > -37 °C only heterogeneous freezing can take place with ice nucleation particles (INP) playing the key role by initiating the freezing process. In mixed-phase clouds supercooled cloud droplets and ice crystals coexist at the same time at temperatures between -35 °C and 0 °C.

Atmos. Chem. Phys. Discuss., doi:10.5194/acp-2016-365, 2016
Manuscript under review for journal Atmos. Chem. Phys.
Published: 9 June 2016

Atmospheric Chemistry and Physics Discussions

Due to the lower saturation vapor pressure over ice compared to water, ice particles grow at the expense of the supercooled droplets (Wegener-Bergeron-Findeisen process; Findeisen 1938 and translated from German and edited by Volken, 2015).

Typically only one out of 10^5 atmospheric particles has the ability to act as an INP (Rogers et al., 1998; DeMott et al., 2010), therefore the abundance of INP is low and ice nucleation is a very selective process. The ability of aerosol particles to act as INP depends on the chemical and physical properties, e.g. water insolubility, particle size, existence of an ice active site (Sullivan et al., 2010), as well as the required chemical bonds and crystallographic properties.

Previous laboratory and field studies have suggested that mineral dust (in several types) is one of the most important INP (e.g. DeMott et al., 2003b; DeMott et al., 2003a; Kamphus et al., 2010; Atkinson et al., 2013; Diehl et al., 2014) because of, in part, its high abundance in the atmosphere (Hoose et al., 2010b). Besides mineral dust organic material from anthropogenic and biological origin is also of particular importance for ice formation (DeMott et al., 2003a; Cziczo et al., 2004b) and also a major component of the atmospheric aerosol in general. Especially biological particles, (e.g. spores, fungi or bacteria) are the most efficient INP at high temperatures (Hoose et al., 2010a). Good ice nucleation ability has also been demonstrated for efflorescent salts (e.g. Abbatt et al., 2006; Wise et al., 2012) and glassy organic material (e.g. Froyd et al., 2010; Murray et al., 2010). Additionally, Tobo et al. (2014) could show that the organic material found in soil dust samples is more important for the ice nucleation ability than the mineral components. Laboratory measurements by Augustin-Bauditz et al. (2016) seem to confirm these findings. The ice nucleation ability of soot particles is currently under controversial discussion: Some studies indicated good ice nucleation ability of soot (e.g. Cozic et al., 2008; Pratt and Prather, 2010; Pratt et al., 2010), but recently Kupiszewski et al. (2016) has shown that black carbon containing particles are depleted in IPR compared to out-of-cloud aerosol.

The aim of the study presented here was the investigation of the chemical composition of IPR in mixed-phase clouds. To achieve this goal, a combination of an ice-selective inlet, the Ice-CVI (Ice Counterflow Virtual Impactor; Mertes et al., 2007), and a single particle mass spectrometer, the ALABAMA (Aircraft-based Laser ABlation Aerosol Mass spectrometer; Brands et al., 2011), was operated at the high alpine research site Jungfraujoch in January/February 2013.

First results of this data set showed a high amount of organic aerosol in both IPR and out-of-cloud aerosol particles. In order to better understand the mass spectral signatures and to be able to assign the individual mass spectra to certain particle types, it was necessary to perform an extensive set of laboratory measurements. Different types of typical atmospheric particles such as biological, mineral and organic anthropogenic particles (with sizes roughly between 100 nm and 3 µm), were studied using single particle mass spectrometry (Kamphus et al., 2008; Brands et al., 2011). The aim of these studies was to identify instrument-specific marker peaks for each particle type. Subsequently these results were applied to the Jungfraujoch data set. The chemical composition of the out-of-cloud aerosol particles is compared to the composition of the sampled IPR and a selected cloud event is compared to an out-of-cloud period having the same air mass origin.

2 Measurements and Methods

Atmos. Chem. Phys. Discuss., doi:10.5194/acp-2016-365, 2016
Manuscript under review for journal Atmos. Chem. Phys.
Published: 9 June 2016

Atmospheric Chemistry and Physics Discussions

2.1 Aerosol Mass Spectrometer

The size-resolved chemical characterization of the aerosol particles was done with the single particle mass spectrometer ALABAMA (Brands et al., 2011). The ALABAMA consists of three parts: inlet system, detection region and ablation/ionization region. An aerodynamic lens (Liu-type; Liu et al., 1995b; Liu et al., 1995a; Kamphus et al., 2008) and a critical orifice form the inlet system of the ALABAMA, which transmits the particles into the vacuum system and focusses the aerosol particles to a narrow beam. At the exit of the aerodynamic lens the particles are accelerated depending to their particle size to a velocity of about 50 - 100 ms^{-1}. For optimal working conditions the critical orifice limits the sampling flow to 80 cm^3min^{-1} and reduces the pressure in the aerodynamic lens to 3.8 hPa. The desired lens pressure was set using a critical orifice with a variable diameter to account for the low ambient pressure at the Jungfraujoch (approx. 650 hPa).

A skimmer separates the inlet system and the detection region (second pumping region). The detection region consists of two continuous wave detection lasers (Blu-Ray laser; InGaN, 405 nm), which are orthogonal to the particle beam. The particles pass through the two laser beams and the scattered light is reflected by an elliptical mirror and detected by a photomultiplier tube (PMT). The particle velocity can be determined from the time period a particle needs to pass both detection lasers. By calibration with particles of known size the vacuum aerodynamic particle diameter (DeCarlo et al., 2004) can be determined from the velocity of the particles. Both detection lasers are also used to trigger the ablation laser (pulsed ND-YAG-Laser, 266 nm, 6 – 8 mJ per pulse, 5.2 ns per pulse, max. 21 Hz). If one particle passes both continuous laser beams the electronic control system (designed and build at the Max Planck Institute for Chemistry, Mainz, Germany) sends out a trigger signal to the ablation laser. Subsequently, the pulsed laser fires and vaporizes the particle partly or completely, ionizing a fraction of the created gas molecules at the same time. The ions are separated in the Z-shaped bipolar time-of-flight mass spectrometer (TOFWERK AG, Switzerland) by their mass-to-charge ratio (m/z) and finally detected by a microchannel plate (MCP). The ALABAMA measures particles with a vacuum aerodynamic diameter in the size range of 100 nm and 3000 nm. The most efficient detection range is between 200 nm and 900 nm.

Additionally, an optical particle counter ("Sky-OPC", Grimm, model 1.129, size diameter range (d): $d > 0.25$ µm, $d < 32$ µm) connected directly to the ALABAMA inlet system measures the size distribution based on the intensity of the light scattered by the particles.

2.2 Single Particle Data Evaluation

The data evaluation was done using the software package CRISP (Concise Retrieval of Information from Single Particles, Klimach, 2012), based on the software IGOR Pro (Version 6, Wave-Metrics), following the procedures described in Roth et al. (2016). CRISP includes mass calibration, the conversion of mass spectra into so-called "stick spectra" by integration over the peak width of the ion signals, as well as different possibilities to sort the mass spectra into groups of clusters of similar spectra. This sorting can be done by the operator or with one of the three implemented cluster algorithms: fuzzy c-means (e.g. Bezdek et al., 1984; Hinz et al., 1999; Huang et al., 2013), k-means (Hartigan and Wong, 1979; Rebotier and Prather, 2007) or minimum spanning tree (Gower and Ross, 1969). Differences between the clustering algorithm k-means and fuzzy c-means and the relevance and impact of some clustering parameters are described in detail in Roth (2014). The data presented in this work are

Atmos. Chem. Phys. Discuss., doi:10.5194/acp-2016-365, 2016
Manuscript under review for journal Atmos. Chem. Phys.
Published: 9 June 2016

Atmospheric Chemistry and Physics Discussions

based on evaluation with the fuzzy c-means algorithm with subsequent manual sorting. The details of the evaluation process are described in the following paragraph:

The result of the clustering depends significantly on the chosen clustering parameters, especially the selected number of start clusters. If this number is too small, rare fragmentation patterns (representing presumably a rare particle type) are possibly not found. For that reason a high number of start clusters was chosen to assure that also seldom fragmentation patterns are considered in the data evaluation (for instance for the out-of-cloud data set from the JFJ campaign 2013 a number of 200 cluster was chosen; for a known particle composition as sampled during the laboratory studies a number of 10 to 50 cluster was chosen depending on the number of spectra). After the mass calibration all spectra were clustered using the fuzzy c-means algorithm (see Table 1 for the adopted clustering parameters). Depending on the chosen clustering parameters, the algorithm yields a specific number of clusters. Each cluster includes a specific number of mass spectra based on the calculated membership and distance (Pearson correlation). From all mass spectra in a cluster an average spectrum is calculated which is used for the identification of the particle type represented by each cluster. All mass spectra which did not fulfill the distance criterion compared to any of the clusters are sorted in the "rest cluster". Afterwards, all average spectra were manually examined with respect to the presence of specific peaks (marker peaks), which help to identify the particle type. At the end all clusters of the same particle type were merged.

2.3 Laboratory measurements

Classification of the different particle types based on typical marker peaks can be done using published single particle mass spectra and the identified corresponding marker peaks from the single particle mass spectrometer literature. However, dependent on ablation laser wavelength and the energy density at the ablation point, these marker peaks are likely to be instrument-specific. Therefore a large set of laboratory reference mass spectra was recorded using the ALABAMA with the objective to determine instrumental specific marker peaks allowing for a more precise particle type classification. These instrument-specific marker peaks are expected to be valid only for the current configuration of the instruments, because parameters like ablation laser wavelength and energy density are likely to influence the ionization efficiency and the ion fragmentation pattern. Because of the high abundance of organic material in the atmospheric aerosol from natural or anthropogenic emissions (Hallquist et al., 2009; Kroll and Seinfeld, 2008; Zhang et al., 2007; Murphy et al., 2006) the focus was put on the distinction of different types of organic material depending on the sources. Additionally, different mineral particle types were investigated in order to differentiate more unambiguously between biological and mineral aerosol (e.g. soil dust). The laboratory measurements include data recorded at the Max Planck Institute for Chemistry in Mainz and at the AIDA (Aerosol Interactions and Dynamics in the Atmosphere; Möhler et al., 2003; Saathoff et al., 2003) chamber at the Karlsruhe Institute for Technology (KIT).

The various particle types were generated for the measurements as suspension or as "washing water" (e.g. from pollen or bacteria), as mechanically dispersed solid particles (e.g. cellulose, minerals or ground leaves), or they were directly produced by combustion (e.g. from biomass burning, fuel exhaust, soot, cigarette smoke or cooking/barbeque emissions). No size selection of the generated particles was done before transferring the particles into the ALABAMA. Coating experiments also were conducted with sulfuric acid and secondary

Atmos. Chem. Phys. Discuss., doi:10.5194/acp-2016-365, 2016
Manuscript under review for journal Atmos. Chem. Phys.
Published: 9 June 2016

organic aerosol (SOA; produced by ozonolysis of α-pinene) coatings on mineral dust particles to mimic atmospheric aging processes.

For the determination of the specific marker peaks only those mass spectra that represented the majority of the different fragmentation patterns were considered. Using these marker peaks biological, mineral and anthropogenic particle types can be differentiated from each other. However, it has to be taken into account that the same particle type can show different fragmentation patterns and that different particle types can also show similar fragmentation patterns. Thus, for precise identification of the particle type, simultaneous measurements of ions of both polarities (anions and cations) by the mass spectrometer is a great advantage, because in many cases the most characteristics signals are only present in one polarity (predominantly in the cation spectra).

2.4 Field studies in mixed-phase clouds

2.4.1 Description of the measurement site

The INUIT-Jungfraujoch campaign took place in January/February 2013 at the High Alpine Research station Jungfraujoch in the Swiss Alps (JFJ, Sphinx Laboratory, 3580 m a.s.l; 7°59'2''E, 46°32'53''N) in the frame work of the DFG (Deutsche Forschungsgemeinschaft)-funded research unit INUIT and the Swiss National Science Foundation-funded project "Interaction of aerosols with clouds and Radiation". It was conducted in cooperation with the CLACE-campaign (Cloud and Aerosol Characterization Experiment) which took place at the same time.

Due to the exposed mountain rim position and the altitude level of the Jungfraujoch the Sphinx Laboratory is mainly situated in the free troposphere in winter time (Lugauer et al., 1998), and is therefore not much affected by local and near-ground emissions. The Jungfraujoch is located in a saddle position between the mountains Mönch and Jungfrau, such that locally the air masses can arrive only from two different directions: From north-west over the Swiss Plateau (wind direction of approx. 315 °) or from south-east over the Inner Alps via the Aletsch Glacier (approx. 135 °) (Hammer et al., 2014). During the measurement campaign the IPR were sampled out of orographic, convective and non-convective clouds.

IPR were sampled by the Ice-CVI from orographic, convective and non-convective clouds. Under cloud conditions the ALABAMA was connected to the Ice-CVI, whereas during cloud-free conditions, the instrument sampled through a heated total aerosol inlet (total; 20 °C; Weingartner et al., 1999). Both inlets were installed on the roof of the Sphinx Laboratory.

The switching between both inlets was done manually, depending on the prevailing cloud conditions

The connection to the two inlet systems limited the maximal particle size of the particles reaching the ALABAMA to approximately 3 µm. The ALABAMA sampled through ¼" stainless steel tubes with different lengths (Ice-CVI to ALABAMA: 126 cm, total to ALABAMA: 261 cm). Particle losses inside the sampling tube were calculated with a modified version of the Particle Loss Calculator (von der Weiden et al., 2009). The transmission efficiency is about 99 % for a particle size between 200 nm and 500 nm and increased with decreasing tube length. The upper 50 %-cut-off of the Ice-CVI is at about 4900 nm and for the total inlet about 3300 nm.

Atmos. Chem. Phys. Discuss., doi:10.5194/acp-2016-365, 2016
Manuscript under review for journal Atmos. Chem. Phys.
Published: 9 June 2016

Atmospheric Chemistry and Physics Discussions

Due to technical problems with the mass spectrometer only the cation mass spectra are available from this field deployment.

2.4.2 Ice particle residual sampling

The Ice-CVI was designed to sample small, fresh ice particles (< 20 µm) out of mixed-phase clouds. A detailed description and instrumental characterization is provided in Mertes et al. (2007), therefore the system is described here only briefly.

The Ice-CVI consists of three main separation sections (omnidirectional inlet, virtual impactor (VI) and pre-impactor (PI)) and a CVI (counterflow virtual impactor). The omnidirectional inlet transfers particles with a particle size up to 20 µm from the aspired air without influences of precipitation and wind. To remove larger particles which entered the inlet system owing to precipitation or wind and to get a defined upper sampling size, the VI is located just below the inlet with an upper transmission limit of 20 µm. Particles larger 20 µm are virtually impacted while smaller particles remain in the sampling flow. Afterwards, ice crystals are separated from the supercooled droplets with the help of the pre-impactor (two-step separation system with 10 µm and 4 µm impaction stages). The impaction plates of the pre-impactor are cooled to ambient temperatures below 0 °C. The small ice particles bounce off the plates and remain in the sample flow whereas the supercooled droplets freeze on the plates upon contact. The transmission efficiencies of the pre-impactor with respect to supercooled droplets and ice crystals are close to 0 % respectively 100 % (Tenberken-Pötzsch et al., 2000; Mertes et al., 2007). Subsequently, the CVI removes all particles smaller than 5 µm, i.e. the interstitial aerosol and smaller supercooled droplets and small ice crystals fragments –that are possibly still in the sampling flow. To accelerate the arriving air flow to 120 ms^{-1} the CVI is located inside a wind tunnel behind the VI and PI. This velocity is required to achieve a size cut of approximately 5 µm. Only particles with sufficient inertia are able to overcome the counterflow inside the CVI. Consequently, only ice crystals with an aerodynamic diameter between 5 µm and 20 µm are sampled. The collected ice crystals are injected into a particle free and dry air inside the CVI, where the ice is completely evaporated. The released particles are the IPR and are transferred to different measurement instruments for physical and chemical characterization.

The sampling principle of the Ice-CVI leads to an enrichment of the sampled particles, which is calculated by the flow ratio before and inside the CVI inlet.

The Ice-CVI samples only ice crystals smaller than 20 µm. Such small ice crystals have grown only by water vapor diffusion and have an age of less than 20 seconds (Fukuta and Takahashi, 1999). Therefore, it is very likely that these ice crystals have formed in the vicinity of the inlets and had only little time to scavenge interstitial aerosol particles, such that the IPR extracted from such fresh ice crystals represent to a high degree to the original IPN (Mertes et al., 2007 and references therein).

A condensation particle counter (CPC, Type 3010, TSI Inc.) is located behind the CVI and measures the INP number concentration

3 Results and Discussion

3.1 Laboratory measurements of reference particles

Atmos. Chem. Phys. Discuss., doi:10.5194/acp-2016-365, 2016
Manuscript under review for journal Atmos. Chem. Phys.
Published: 9 June 2016

Atmospheric Chemistry and Physics Discussions

A summary of all investigated particles types (subdivided into three classes "biological", "mineral", and "anthropogenic") is provided in Table 3 with their specific marker peaks. There are certain particle types where the number of mass spectra containing specific and unique marker peaks is relatively low (e.g. grounded maple leaves, brown coal, desert dust and volcano dust). This results partially in high uncertainties in the identification of these particle types in ambient data

Table 3 shows that some particle types belonging to one class show similarities in their marker peaks. For instance, the biological particle types bacteria and pollen have very similar fragmentation patterns (m/z -45 ($[C_2H_5O/CHO_2]^-$), -63 (PO_2^-), -71 ($[C_4H_7O/C_3H_3O_2]^-$), -79 (PO_3^-) and 47 (PO^+); fragments of oxidized organic carbon and phosphate). Also cellulose (microcrystalline) and ground leaves exhibit similar marker peaks (m/z 18 (NH_4^+)/(H_2O^+), 30 ($[CH_4N]^+$/$[COH_2]^+$), 58 ($[C_3H_8N]^+$/$[C_3H_6O]^+$); fragments indicating an amine-like or oxidized organic structure). Thus, it is not possible to distinguish here between different types of biological aerosol particles. Nevertheless, in general the identification of biological aerosol with the help of characteristic marker peaks is possible.
Additionally, also similarities between particle types from two different classes occur: Sea salt (industrial produced; Sigma Aldrich) and particles from cooking/barbecue emissions have similar fragmentation patterns in the cation spectra (m/z 46, 81, 83, 97, fragments of sodium/potassium components).
Cigarette smoke produced in two different ways was also measured: smoldering cigarette smoke and cigarette smoke which was firstly inhaled. The particles from smoke after inhalation do not show any PAH fragmentation. But both types of cigarette smoke could not be unambiguously identified.
Some rare fragmentation patterns from pollen and biomass burning particles show similarities within the cation spectra (only one sodium (m/z 23) and potassium (m/z 39) peak). Summarizing, it was found that in general the presence of both polarities is of great importance for an unambiguous identification of a specific particle type. Only few particle types, as for example the anthropogenically produced particle types show distinct marker peaks the cation spectra that are sufficient for identification.

3.2 Results on IPR composition and out-of-cloud aerosol at the Jungfraujoch

3.2.1 Identified Particle Types

Altogether 71064 background aerosol particles were analyzed during 217 h measurement time and 595 IPR during 111 h measurement time. For the identification of specific particle types the marker peaks that resulted from the laboratory studies were applied to the Jungfraujoch data. Although, as mentioned above, the presence of both polarities allows in general for a better classification, the application of the marker peaks only for the cations yielded also useful results, because many distinguishing characteristics are found in the cation spectra (Table 3). In this way 13 different particle types were identified. The average spectra of each particle type with the highlighted marker peaks are shown in Fig. 1.

The particle types "biomass burning" and "soot" show both the typical C_n-fragmentation (C_1 – C_7, m/z 12 … 84) and can be distinguished by the presence of the peak at m/z 39 (K^+) in the cation spectra of the particles from biomass burning.

Atmos. Chem. Phys. Discuss., doi:10.5194/acp-2016-365, 2016
Manuscript under review for journal Atmos. Chem. Phys.
Published: 9 June 2016

Atmospheric Chemistry and Physics Discussions

Two different fragmentation patterns of biological particles were found during the campaign. One type shows the marker peaks at m/z 18, 30, 58 and 59, which indicates an amine-like or oxidized organic structure. The other one shows the marker peak at m/z 47 (PO^+).
Additionally, soil dust was identified based on the laboratory studies. It is characterized by the presence of mineral components mixed with organic, biological material (e.g. peaks at m/z 18, 30, 58 and 47 point to biological components).
The laboratory data have shown that particles produced from cooking emissions and sea salt particles have the same cation fragmentation pattern. Thus, both particle types cannot be distinguished in this data set and therefore were merged.

Also from the particle type "aged material" two different fragmentation patterns were found. The first one shows peaks at m/z 27 and 43 (fragments of organic material related to secondary organic aerosol) with a high relative intensity. The other one shows peaks at m/z 92, 108 and 165, which points to nitrate and sulfate containing compounds.

The particle types "engine exhaust" and "PAH" were identified through the corresponding reference spectra and marker peaks from the laboratory studies.

The particle type "industrial metals" is marked by peaks of metal ions typically occurring in urban or industrial emissions (e.g. m/z 51/67 (V^+/VO^+), m/z 54/56 (Fe^+), m/z 55 (Mn^+), m/z 58/60 (Ni^+), m/z 59 (Co^+) and m/z 63/65 (Cu^+) (de Foy et al., 2012)). Chromium and nickel containing particles might also originate from contamination by the stainless steel tubes. But due to the low flow velocity and the laminar flow inside the tubes the production of particles by abrasion from the tube walls through collision of the aerosol particles with the inner wall of the tubes can be neglected. Another source of such contamination might be the valves that might mechanically produce particles during opening and closing. However, such particles are expected to be detected by the mass spectrometer within a few seconds after operation of a valve which was not the case. Thus we consider these particles to be real ambient atmospheric particles.
Lead containing particles show the typical isotope pattern of lead (m/z 208, 207, 206, 204) and are internally mixed with metallic or organic components. Previous measurements at the JFJ have shown that lead containing particles were found in the IPR (Cziczo et al., 2009; Ebert et al., 2011). However, the main component of this particle type is organic or metallic origin. Thus it can be assumed that lead is only contained in small amounts in these particles. Using data from the same experiment, Worringen et al. (2015) have shown that two types of lead particles occurred in the IPR selected by the Ice-CVI during the INUIT-JFJ campaign: large homogeneous lead particles and small particles with lead inclusions. The authors concluded that only the homogeneous lead particles are artifacts produced by mechanical abrasion from the surface of the impaction plates of the Ice-CVI. Therefore, the lead containing particles described here are not considered as artifacts of the Ice-CVI.
Mineral dust particles ("minerals") were also found in the aerosol particles sampled during the JFJ campaign. This particle type was identified based on the marker peaks from the laboratory studies as well.
The types "K dominated" and "Na + K" are subcategories of the type "other", but are not clearly assignable to a certain particle type. As we inferred from the laboratory studies both particle types could originate from biological particles (e.g. pollen) or from biomass burning. On the other hand it is also possible that the "K

dominated"-type is a fragmentation pattern of an inorganic salt (e.g. K_2SO_4). An unambiguous classification of these particle types from cation spectra only is not possible.
Most of these particle types do not represent pure particles like those investigated during the laboratory studies. The particles contain also other substances (as can be seen in the mass spectra) but here the most prominent marker peaks were used to identify the dominating particle type
The type "others" includes all spectra which could not be unambiguously identified as one of the introduced particle types. This may partly be due to missing reference spectra, such that a further extension of the reference data base will allow for an identification of particles in the "other" fraction, but also due to complex mixtures of particles that cannot be identified here, especially because the anions were not available.

3.2.2 IPR composition compared to out-of-cloud aerosol particles

Figure 2 shows the relative abundance of the identified particle types in all aerosol particles sampled out-of-cloud in comparison to all sampled IPR during all cloud periods.

In comparison to the out-of-cloud aerosol the IPR ensemble shows a higher relative amount of particles from natural sources (e.g. primary biological particles and sea salt, but also biomass burning particles generated from forest fires can be related to natural sources). Between about 43 and 50 % of the identified particle types can be attributed to natural sources; the uncertainty range is mainly due to the inability to separate between sea salt particles and cooking emissions. Additionally, the IPR has a higher fraction of lead containing particles (7 %), industrial metals (4 %) and particles from engine exhaust (6 %) in comparison to the composition of the out-of-cloud aerosol. This enrichment of lead-containing particles measured at the JFJ was also shown by Kamphus et al. (2010) and Ebert et al. (2011). The out-of-cloud aerosol shows a higher fraction of aged material (30 %), combustion particles (12 % PAH/soot; 10 % biomass burning) and potassium-dominated particles (11 %). From the absence of potassium-dominated particles as well as the absence of biomass burning particles within the IPR ensemble, together with the occurrence of the same fragmentation pattern in the laboratory data for biomass burning particles, it can be surmised that the potassium-dominated type possibly originates also from biomass burning particles. On the other hand potassium containing salts also may be the source of these particles, which are not acting as INP (Twohy and Poellot, 2005).

The detection of potassium in laser ablation mass spectrometry is very efficient. In a laser ablation mass spectrometer the intensity of the peaks depends on the ionization efficiency. Potassium is easily ionized, such that a small amount of potassium in a particle results in a large peak and will suppress the peak intensity of other components with lower ionization efficiencies.

It is unexpected that the IPR ensemble contains particles from engine exhaust but not particles from biomass burning, because the latter are also assumed to have good ice nucleation ability (Kamphus et al., 2010; Twohy et al., 2010; Pratt et al., 2011; Prenni et al., 2012). Additionally, lead-containing particles and particles from engine exhaust were found in INP composition (Kamphus et al., 2010; Corbin et al., 2012). Due to the finding that the same relative abundance of the particle type "PAH/soot" is found in both particle populations (12 %) and the finding that biomass burning particles as well as particles from engine exhaust show an organic fragmentation pattern, further research is necessary to determine which specific property of these particle types enables their ice nucleation ability.

Atmos. Chem. Phys. Discuss., doi:10.5194/acp-2016-365, 2016
Manuscript under review for journal Atmos. Chem. Phys.
Published: 9 June 2016

There are only a few comparable single particle measurements reported in the literature: Measurements with the ATOFMS (Aerosol Time-of-Flight Mass Spectrometer) at the JFJ (Cziczo et al., 2009), and also aircraft measurements over North America show an amount of 5 and 10 % lead-containing particles at the out-of-cloud aerosol (Murphy et al., 2007). However, only a minor amount of minerals and fly ash was found at the Storm Peak Laboratory (SPL; 3200 m a.sl.) in northern Colorado (DeMott et al., 2003a). In agreement with our data, measurements from SPL show also organic material (e.g. biomass burning particles, aged material, and PAH/soot; see Fig. 2) as the major compound of the out-of-cloud aerosol (DeMott et al., 2003a; Cziczo et al., 2004a).

The finding that the particle abundance in the IPR is different from that in the out-of-cloud aerosol confirms the assumption that scavenging of interstitial aerosol particles plays only a minor role for the composition of the IPR, because if interstitial particle scavenging dominated, the IPR composition would look similar to that of the out-of-cloud aerosol. The presence of aged material (in low percentage) in the IPR may be explained by aerosol scavenging, but shows the limited influence of this process on IPR composition (3 % in IPR in contrast to 30 % in out-of-cloud-aerosol). This is what was aimed for by designing the Ice-CVI to sample only small, freshly produced ice crystals with sizes below 20 µm.

From the observation that certain particle types are enriched in the IPR ensemble whereas other are less abundant, some general statements on the ice nucleation ability of these particle types can be made:

High ice nucleation ability can be inferred for soil dust, minerals, sea salt/cooking emissions, particles from engine exhaust, lead containing particles and industrial metals. Lower ice nucleation ability can be assumed for aged material, potassium-dominated particles and particles from biomass burning.

For those particle types that occurred in the same percentage in the out-of-cloud aerosol and in the IPR ensemble, as PAH/soot particles and biological particles, a precise statement regarding their ice nucleation ability under the prevailing meteorological conditions cannot be inferred from this data set. The finding that biological particles are of minor importance during wintertime at the Jungfraujoch is supported by a recent study using light-induced fluorescence that showed that most fluorescent particles were mineral dust and not biological particles (Crawford et al., 2016).

3.2.3 Size resolved analysis

As mentioned above, the ALABAMA also allows for a size resolved chemical analysis of the sampled aerosol particles. Additional size information can be obtained by the OPC that was operated in parallel to the ALABAMA at the same sampling line. Figure 3 shows the size distribution of IPR and the out-of-cloud aerosol particles analyzed by ALABAMA (a and c) and those detected by the Sky-OPC (b and f). The ALABAMA data include only particles of which a mass spectrum was obtained. The size distribution measured with the Sky-OPC represents all registered particles at the total inlet and the Ice-CVI, respectively.

The size distribution of the IPR analyzed by ALABAMA (Fig. 3a, right ordinates) shows in comparison to the out-of-cloud aerosol (Fig. 3b) a wider distribution, especially to the larger particles size ($d > 1000$ nm). It must be emphasized here that the ALABAMA size distribution does not represent the "real" ambient size distribution but is a function of the detection and ionization efficiency, which is optimal around 400 nm. Therefore, the

Atmos. Chem. Phys. Discuss., doi:10.5194/acp-2016-365, 2016
Manuscript under review for journal Atmos. Chem. Phys.
Published: 9 June 2016

ambient size distributions measured with the Sky-OPC (Figs. 3b and 3d) do not show a maximum for particle diameters above 250 nm (the lower detection limit of the Sky-OPC), but a decrease of the particle number concentration with increasing particle diameter.

The size-resolved chemical composition of the IPR (Fig. 3a) does not show a clear relationship between size distribution and particle type, partly caused by the low counting statistics. In the lowest size bin (100 – 200 nm) the fraction of biological and PAH/soot is highest, while mineral particles (minerals and soil dust) are enhanced in the size range between 300 nm and 800 nm. Industrial metal particle are only present in the size range from 300 nm up to approximately 1800 nm.

The out-of-cloud aerosol shows an increased number of biological particles between 200 and 400 nm and larger than 1000 nm. The number of potassium-dominated particles is enhanced up to about 600 nm while the highest number of biomass burning particles is found in the size range from 300 nm up to 1000 nm. Thus, the potassium-dominated particles seem to originate more likely from biological particles or from inorganic salts than from biomass burning. In contrast, the number of 'Na+K'-particles is enriched at higher sizes (> 500 nm), suggesting another source for this particle type.

According to Fig. 3b the larger sized IPR (d > 1 µm) are present at a higher fraction of the total particle number than the same sizes are in the out-of-cloud aerosol (Fig. 3d). This confirms the assumption that larger particles are better INP.

A comparison of the absolute numbers of particles and the calculation of an activity curve is not possible, because the out-of-cloud aerosol particles and the IPR (inside clouds) were measured, per definition, at different times.

3.2.4 Case study of a selected cloud event

The comparison of all sampled particles from the out-of-cloud aerosol with all sampled IPR exhibits significant differences between both compositions. However a comparison extending over the entire data set is limited as different meteorological conditions or air mass origins are included. For a closer look at the chemical composition of the out-of-cloud aerosol and the IPR, a comparison of two shorter sample periods representing both aerosol types was performed. To find appropriate time periods with comparable meteorological conditions, at first temperature, relative humidity, wet-bulb temperature, and wind direction were inspected. Two closely spaced sample periods were chosen, one in clouds and the other outside, with nearly the same average temperature, relative humidity and wind direction. The meteorological parameters for the two sample periods are depicted in Fig. 4 with the corresponding air mass origin back trajectories given in Fig. 5. For this purpose the HYSPLIT model was adopted (Hybrid Single Particle Langrangian Integrated Trajectory Model, National Oceanic and Atmospheric Administration; Draxler and Rolph, 2015; Rolph, 2015) with access to the meteorological data set GDAS (Global Data Assimilation; start height: 3580 m a.s.l.; calculated time: 72 h back; start time: end of the current sampling period).

The back trajectory calculations show that the air masses of both sample periods have similar, but not completely the same origin, and –besides the two excursions to higher altitudes– also a similar altitude profile of the

Atmos. Chem. Phys. Discuss., doi:10.5194/acp-2016-365, 2016
Manuscript under review for journal Atmos. Chem. Phys.
Published: 9 June 2016

Atmospheric Chemistry and Physics Discussions

trajectories. The air masses arrived while rising-towards the measurement platform from north-western region via France.

Figure 6 shows the composition of the out-of-cloud aerosol and the IPR ensemble during these two sampling times. Although the sampling conditions during both periods were very similar, the composition of these ensembles significantly differs. The IPR ensemble shows a high content of primary, natural material (74 – 77 %; biological particles, soil dust, minerals and sea salt/cooking emissions). In comparison to that, the out-of-cloud aerosol contains a higher fraction of particles from biomass burning (22 %) and potassium-dominated particles (22 %). These findings agree with the general statement that natural primary aerosol such as biological particles, soil dust or minerals serve as typical ice nucleators. The large relative amount of biological particles in the IPR samples exceeds that of the total IPR sample (Fig. 2), whereas for the out-of-cloud sample it is smaller (cf. Fig. 2). Here the variability due to different sampling times, temperatures, and air mass origins may play a role. The high amount of particles from biomass burning in the out-of-cloud aerosol indicates that the air masses were most likely influenced by local emissions shortly before arrival at the measurement station, but still these biomass burning particles are not found in the IPR ensemble.

It has further to be noted that one air mass during the out-of-cloud sample period has a different pressure history than the others: It rose up to about 400 hPa at about 50 h (Fig. 5) prior to the measurements and rapidly descended again at 30 h prior to the measurements. A closer look at the chemical composition of the particles in this air mass shows that mostly PAH/soot particles were sampled. A possible explanation might be that the aerosol particles in this air mass were removed by cloud formation or by wet removal during the uplift, and that after the downward motion the air mass picked up the local emissions from traffic or combustion, such that –in contrast to the other air masses– the combustion-related particles dominate.

Since the differences within the chemical composition of both sampling periods cannot be explained by differences in air mass origin, we assume that the difference between the out-of-cloud aerosol and the IPR regarding the chemical composition is mainly caused by the ice nucleation ability of the particles at the prevailing meteorological conditions during this sample periods. At temperatures around -20 °C biological particles, soil dust, minerals, sea salt/cooking emissions, PAH/soot and lead containing particles have good ice nucleation ability. Another conclusions is that here the scavenging of interstitial aerosol particles cannot explain the observed differences in composition.

4 Summary

We have conducted laboratory measurements of various types of aerosol particles in order to obtain references mass spectra for the single particle mass spectrometer ALABAMA. The results show that there are different particle classes, which can be unambiguously differentiated from each other by using specific marker peaks. The derived specific marker peaks can be applied to interpret field data where ice residuals from mixed-phase clouds were extracted by an Ice-CVI and analyzed by the mass spectrometer. The comparison of the chemical composition of the out-of-cloud aerosol particles and the IPR measured during the INUIT-JFJ campaign 2013 revealed significant differences within both ensembles. Certain particles types were found to be enriched in the IPR ensemble in comparison to the out-of-cloud aerosol. From this we can determine ambient atmospheric particle types that preferably act as ice nucleating particles under the prevailing meteorological conditions at this

time. The high ice nucleation ability of lead containing particles (Cziczo et al., 2009), minerals (e.g. Kamphus et al., 2010; Hoose et al., 2010b; Hartmann et al., 2011; Hoose and Möhler, 2012; Atkinson et al., 2013), soil dust (Tobo et al., 2014), and sea salt/cooking emissions (Wilson et al., 2015) could be confirmed. Additionally, particles from engine exhaust (Corbin et al., 2012), and industrial metals can be assumed as ice-active. It has been also reported that particles from biomass burning are efficient ice nucleating particles (Twohy et al., 2010; Pratt et al., 2011; Prenni et al., 2012). However, during the measurements at the JFJ 2013 no particles from biomass burning were found in the IPR ensemble. In contrast to the IPR, the ensemble of the out-of-cloud aerosol particles was dominated by aged material and particles produced by combustion (10 % biomass burning and 12 % PAH/soot). The size distribution of both aerosol types have shown that the relative number of particles with a larger vacuum aerodynamic diameter measured with the ALABAMA ($d > 1000$ nm) is higher in the IPR ensemble than in the out-of-cloud aerosol. Additionally, a comparison between both particle populations was made for two closely spaced measurement periods. Although all meteorological conditions, e.g. temperature, relative humidity and wind direction (air mass origin) were similar, the chemical composition of the IPR was found to be different to that of the out-of-cloud aerosol. In comparison to the out-of-cloud aerosol particles, the IPR mainly consist of biological particles (49 %) and soil dust (19 %) whereas the ensemble of the out-of-cloud aerosol particles is enriched with particles from biomass burning (22 %) and potassium dominated particles (22 %). Because the percentage of biological particles is similar in the out of-cloud and IPR ensembles we can conclude that biological particles are ice-active at temperatures around -20 °C (temperature range between -27 °C and -6 °C over the whole measurement campaign). On the other hand, the case study indicates also a high event-to-event variability. The high amount of particles from biomass burning, which are not found in the IPR, indicates an influence of local emissions. This case study confirmed that the observed general differences between IPR and aerosol particle composition is not due to different air mass origin or meteorological conditions but reflects the different ice nucleation abilities of certain atmospheric particles types. The data also show that laboratory results on the ice nucleation ability of certain particles types (e.g., mineral dust and other primary particles; Möhler et al., 2007; Hoose and Möhler, 2012; Atkinson et al., 2013; Augustin-Bauditz et al., 2014; Hiranuma et al., 2015) can at least partly by transferred to ambient atmospheric data. Some of the IPR results may be influenced by scavenging of interstitial aerosol particles by the ice crystals, but this process cannot explain the differences between the composition of the IPR and the out-of-cloud aerosol.

Acknowledgements

This work was supported by the DFG projects for 1525 (INUIT), SPP 1294 (HALO, grant ME 3524/1-2), the Max Planck Society, the European Union Seventh Framework Programme (FP7/2007-2013) under grant agreement no 2662254 (ACTRIS TNA) and the Swiss National Science Foundation (200021L 135356).

The authors gratefully acknowledge the NOAA Air Resources Laboratory (ARL) for the provision of the HYSPLIT transport and dispersion model and/or READY website (http://www.ready.noaa.gov) used in this publication.

We would like to thank Swiss Meteorological Institute (MeteoSwiss) for providing meteorological measurements and the International Foundation High Altitude Research Station Junfgraujoch and Gornergrat (HFSJG) for the opportunity to perform experiments at the Jungfraujoch. Additional thanks go to Oliver Appel

(MPIC Mainz) for help with the OPC data evaluations, to Oliver Schlenczek (University Mainz) for cloud observation at the JFJ and to Udo Kästner (TROPOS) for his help during the measurements at the JFJ.

References

Abbatt, J. P., Benz, S., Cziczo, D. J., Kanji, Z., Lohmann, U., and Möhler, O.: Solid ammonium sulfate aerosols as ice nuclei: a pathway for cirrus cloud formation, Science, 313, 1770-1773, 2006.

Atkinson, J. D., Murray, B. J., Woodhouse, M. T., Whale, T. F., Baustian, K. J., Carslaw, K. S., Dobbie, S., O'Sullivan, D., and Malkin, T. L.: The importance of feldspar for ice nucleation by mineral dust in mixed-phase clouds, Nature, 498, 355-358, 2013.

Augustin-Bauditz, S., Wex, H., Kanter, S., Ebert, M., Niedermeier, D., Stolz, F., Prager, A., and Stratmann, F.: The immersion mode ice nucleation behavior of mineral dusts: A comparison of different pure and surface modified dusts, Geophysical Research Letters, 41, 7375-7382, 2014.

Augustin-Bauditz, S., Wex, H., Denjean, C., Hartmann, S., Schneider, J., Schmidt, S., Ebert, M., and Stratmann, F.: Laboratory-generated mixtures of mineral dust particles with biological substances: Characterization of the particle mixing state and immersion freezing behavior, accepted by Atmospheric Chemistry and Physics, doi:10.5194/acpd-15-29639-2015, 2016.

Bezdek, J. C., Ehrlich, R., and Full, W.: FCM: The fuzzy c-means clustering algorithm, Computers & Geosciences, 10, 191-203, 1984.

Brands, M., Kamphus, M., Böttger, T., Schneider, J., Drewnick, F., Roth, A., Curtius, J., Voigt, C., Borbon, A., Beekmann, M., Bourdon, A., Perrin, T., and Borrmann, S.: Characterization of a Newly Developed Aircraft-Based Laser Ablation Aerosol Mass Spectrometer (ALABAMA) and First Field Deployment in Urban Pollution Plumes over Paris During MEGAPOLI 2009, Aerosol Science and Technology, 45, 46-64, 2011.

Cantrell, W., and Heymsfield, A.: Production of Ice in Tropospheric Clouds: A Review, in: Bulletin of the American Meteorological Society, 6, 795-807, 2005.

Corbin, J. C., Rehbein, P. J. G., Evans, G. J., and Abbatt, J. P. D.: Combustion particles as ice nuclei in an urban environment: Evidence from single-particle mass spectrometry, Atmospheric Environment, 51, 286-292, 2012.

Cozic, J., Mertes, S., Verheggen, B., Cziczo, D. J., Gallavardin, S. J., Walter, S., Baltensperger, U., and Weingartner, E.: Black carbon enrichment in atmospheric ice particle residuals observed in lower tropospheric mixed phase clouds, Journal of Geophysical Research-Atmospheres, 113, D15209, 2008.

Crawford, I., Llloyd, G., Herrmann, E., Hoyle, C. R., Bower, K. N., Connolly, P. J., Flynn, M. J., Kaye, P. H., Choularton, T. W., and Gallagher, M. W.: Observations of fluorescent aerosol-cloud interactions in the free troposphere at the High-Altitude Research Station Jungfraujoch, Atmospheric Chemistry and Physics, 16, 2273-2284, 2016.

Cziczo, D. J., DeMott, P. J., Brooks, S. D., Prenni, A. J., Thomson, D. S., Baumgardner, D., Wilson, J. C., Kreidenweis, S. M., and Murphy, D. M.: Observations of organic species and atmospheric ice formation, Geophysical Research Letters, 31, L12116, 2004a.

Cziczo, D. J., Murphy, D. M., Hudson, P. K., and Thomson, D. S.: Single particle measurements of the chemical composition of cirrus ice residue during CRYSTAL-FACE, Journal of Geophysical Research-Atmospheres, 109, D04201, 2004b.

Cziczo, D. J., Stetzer, O., Worringen, A., Ebert, M., Weinbruch, S., Kamphus, M., Gallavardin, S. J., Curtius, J., Borrmann, S., Froyd, K. D., Mertes, S., Möhler, O., and Lohmann, U.: Inadvertent climate modification due to anthropogenic lead, Nature Geoscience, 2, 333-336, 2009.

de Foy, B., Smyth, A. M., Thompson, S. L., Gross, D. S., Olson, M. R., Sager, N., and Schauer, J. J.: Sources of nickel, vanadium and black carbon in aerosols in Milwaukee, Atmospheric Environment, 59, 294-301, 2012.

DeCarlo, P. F., Slowik, J. G., Worsnop, D. R., Davidovits, P., and Jimenez, J. L.: Particle Morphology and Density Characterization by Combined Mobility and Aerodynamic Diameter Measurements. Part 1: Theory, Aerosol Science and Technology, 38, 1185-1205, 2004.

DeMott, P. J., Cziczo, D. J., Prenni, A. J., Murphy, D. M., Kreidenweis, S. M., Thomson, D. S., Borys, R., and Rogers, D. C.: Measurements of the concentration and composition of nuclei for cirrus formation, Proceedings of the National Academy of Sciences of the United States of America, 100, 14655-14660, 2003a.

DeMott, P. J., Sassen, K., Poellot, M. R., Baumgardner, D., Rogers, D. C., Brooks, S. D., Prenni, A. J., and Kreidenweis, S. M.: African dust aerosols as atmospheric ice nuclei, Geophysical Research Letters, 30, 1-4, 2003b.

DeMott, P. J., Prenni, A. J., Liu, X., Kreidenweis, S. M., Petters, M. D., Twohy, C. H., Richardson, M. S., Eidhammer, T., and Rogers, D. C.: Predicting global atmospheric nuclei distributions and their impacts on climate, Proceedings of the National Academy of Sciences of the United States of America, 107, 11217-11222, 2010.

Diehl, K., Debertshäuser, M., Eppers, O., Schmithüsen, H., Mitra, S. K., and Borrmann, S.: Particle surface area dependence of mineral dust in immersion freezing mode: investigations with freely suspended drops in an acoustic levitator and a vertical wind tunnel, Atmospheric Chemistry and Physics 14, 12343-12355, 2014.

Draxler, R. R., and Rolph, G. D.: HYSPLIT (HYbrid Single-Particle Lagrangian Integrated Trajectory) Model Access via NOAA ARL READY Website (http://ready.arl.noaa.gov/HYSPLIT.php), NOAA Air Resources Laboratory, Silver Spring MD, 2015.

Ebert, M., Worringen, A., Benker, N., Mertes, S., Weingartner, E., and Weinbruch, S.: Chemical composition and mixing-state of ice residuals sampled within mixed phase clouds, Atmospheric Chemistry and Physics, 11, 2805-2816, 2011.

Findeisen 1938, W., and translated from German and edited by Volken, E., Giesche, A. M., and Brönnimann, S.: Colloidal meteorological processes in the formation of precipitation, Meteorologische Zeitschrift, 24, 443-454, 10.1127/metz/2015/0675, 2015.

Froyd, K. D., Murphy, D. M., Lawson, P., Baumgardner, D., and Herman, R. L.: Aerosols that form subvisible cirrus at the tropical tropopause, Atmospheric Chemistry and Physics, 10, 209-218, 2010.

Fukuta, N., and Takahashi, T.: The Growth of Atmospheric Ice Crystals: A Summary of Findings in Vertical Supercooled Cloud Tunnel Studies, Journal of the Atmospheric Sciences, 56, 1963-1979, 1999.

Gower, J. C., and Ross, G. J. S.: Minimum Spanning Trees and Single Linkage Cluster Analysis, Journal of the Royal Statistical Society, 18, 54-64, 1969.

Hallquist, M., Wenger, J. C., Baltensperger, U., Rudich, Y., Simpson, D., Claeys, M., Dommen, J., Donahue, N. M., George, C., Goldstein, A. H., Hamilton, J. F., Herrmann, H., Hoffmann, T., Iinuma, Y., Jang, M., Jenkin, M. E., Jimenez, J. L., Kiendler-Scharr, A., Maenhaut, W., McFiggans, G., Mentel, T. F., Monod, A., Prévot, A. S. H., Seinfeld, J. H., Surratt, J. D., Szmigielski, R., and Wildt, J.: The formation, properties and impact of

secondary organic aerosol: current and emerging issues, Atmospheric Chemistry and Physics, 9, 5155-5236, 2009.

Hammer, E., Bukowiecki, N., Gysel, M., Jurányi, Z., Hoyle, C. R., Vogt, R., Baltensperger, U., and Weingartner, E.: Investigation of the effective peak supersaturation for liquid-phase clouds at the high-alpine site Jungfraujoch, Switzerland (3580 m a.s.l.), Atmospheric Chemistry and Physics, 14, 1123-1139, 2014.

Hartigan, J. A., and Wong, M. A.: Algorithm AS 136: A K-Means Clustering Algorithm, Journal of the Royal Statistical Society, 28, 200-108, 1979.

Hartmann, S., Niedermeier, D., Voigtländer, J., Clauss, T., Shaw, R. A., Wex, H., Kiselev, A., and Stratmann, F.: Homogeneous and heterogeneous ice nucleation at LACIS: operating principle and theoretical studies, Atmospheric Chemistry and Physics, 11, 1753-1767, 2011.

Hinz, K.-P., Greweling, M., Drews, F., and Spengler, B.: Data Processing in On-line Laser Mass Spectrometry of Inorganic, Organic, or Biological Airborne Particles, American Society for Mass Spectrometry, 10, 648-660, 1999.

Hiranuma, N., Möhler, O., Yamashita, K., Tajiri, T., Saito, A., Kiselev, A., Hoffmann, N., Hoose, C., Jantsch, E., Koop, T., and Murakami, M.: Ice nucleation by cellulose and its potential contribution to ice formation in clouds Nature Geoscience, 8, 273-277, 2015.

Hoose, C., Kristjánsson, J. E., and Burrows, S. M.: How important is biological ice nucleation in clouds on a global scale?, Environmental Research Letters, 5, 024009, 2010a.

Hoose, C., Kristjánsson, J. E., Chen, J.-P., and Hazra, A.: A Classical-Theory-Based Parameterization of Heterogeneous Ice Nucleation by Mineral Dust, Soot, and Biological Particles in a Global Climate Model, Journal of the Atmospheric Sciences, 67, 2483-2503, 10.1175/2010jas3425.1, 2010b.

Hoose, C., and Möhler, O.: Heterogeneous ice nucleation on atmospheric aerosols: a review of results from laboratory experiments, Atmospheric Chemistry and Physics, 12, 9817-9854, 2012.

Huang, M., Hao, L., Guo, X., Hu, C., Gu, X., Zhao, W., Wang, Z., Fang, L., and Zhang, W.: Characterization of secondary organic aerosol particles using aerosol laser time-of-flight mass spectrometer coupled with FCM clustering algorithm, Atmospheric Environment, 64, 85-94, 2013.

Kamphus, M., Ettner-Mahl, M., Brands, M., Curtius, J., Drewnick, F., and Borrmann, S.: Comparison of Two Aerodynamic Lenses as an Inlet for a Single Particle Laser Ablation Mass Spectrometer, Aerosol Science and Technology, 42, 970-980, 2008.

Kamphus, M., Ettner-Mahl, M., Klimach, T., Drewnick, F., Keller, L., Cziczo, D. J., Mertes, S., Borrmann, S., and Curtius, J.: Chemical composition of ambient aerosol, ice residues and cloud droplet residues in mixed-phase clouds: single particle analysis during the Cloud and Aerosol Characterization Experiment (CLACE 6), Atmospheric Chemistry and Physics, 10, 8077-8095, 2010.

Klimach, T.: Chemische Zusammensetzung der Aerosole - Design und Datenauswertung eines Einzelpartikel-Laserablationsmassenspektrometers, PhD thesis, University of Mainz, Germany, urn:nbn:de:hebis:77-33547, 2012.

Kroll, J. H., and Seinfeld, J. H.: Chemistry of secondary organic aerosol: Formation and evolution of low-volatility organics in the atmosphere, Atmospheric Environment, 42, 3593-3624, 2008.

Kupiszewski, P., Zanatta, M., Mertes, S., Vochezer, P., Llloyd, G., Schneider, J., Schenk, L., Schnaiter, M., Baltensperger, U., and Weingartner, E.: Ice residual properties in mixed-phase clouds at the high-alpine Jungfraujoch site, submitted to Journal Geophysical Research 2016.

Liu, P., Ziemann, P. J., Kittelson, D. B., and McMurry, P. H.: Generating Particle Beams of Controlled Dimensions and Divergence: II. Experimental Evaluation of Particle Motion in Aerodynamic Lenses and Nozzle Expansions, Aerosol Science and Technology, 22, 314-324, 1995a.

Liu, P., Ziemann, P. J., Kittelson, D. B., and McMurry, P. H.: Generating Particle Beams of Controlled Dimensions and Divergence: I. Theory of Particle Motion in Aerodynamic Lenses and Nozzle Expansions, Aerosol Science and Technology, 22, 293-313, 1995b.

Lohmann, U., and Feichter, J.: Global indirect aerosol effects: a review, Atmospheric Chemistry and Physics, 5, 715-737, 2005.

Lugauer, M., Baltensperger, U., Furger, M., Gäggeler, H. W., Jost, D. T., Schwikowski, M., and Wanner, H.: Aerosol transport to the high Alpine sites Jungfraujoch (3454m asl) and Colle Gnifetti (4452m asl), Tellus, 50B, 76-92, 1998.

Mertes, S., Verheggen, B., Walter, S., Connolly, P., Ebert, M., Schneider, J., Bower, K. N., Cozic, J., Weinbruch, S., Baltensperger, U., and Weingartner, E.: Counterflow Virtual Impactor Based Collection of Small Ice Particles in Mixed-Phase Clouds for the Physico-Chemical Characterization of Tropospheric Ice Nuclei: Sampler Description and First Case Study, Aerosol Science and Technology, 41, 848-864, 2007.

Möhler, O., Stetzer, O., Schaefers, S., Linke, C., Schnaiter, M., Tiede, R., Saathoff, H., Krämer, M., Mangold, A., Budz, P., Zink, P., Schreiner, J., Mauersberger, K., Haag, W., Kärcher, B., and Schurath, U.: Experimental investigation of homogeneous freezing of sulphuric acid particles in the aerosol chamber AIDA, Atmospheric Chemistry and Physics, 3, 211-223, 2003.

Möhler, O., DeMott, P. J., Vali, G., and Levin, Z.: Microbiology and atmospheric processes: the role of biological particles in cloud physics, Biogeoscience, 4, 1059-1071, 2007.

Murphy, D. M., Cziczo, D. J., Froyd, K. D., Hudson, P. K., Matthew, B. M., Middlebrook, A. M., Peltier, R. E., Sullivan, A., Thomson, D. S., and Weber, R. J.: Single-particle mass spectrometry of tropospheric aerosol particles, Journal of Geophysical Research, 111, D23S32, 2006.

Murphy, D. M., Hudson, P. K., Cziczo, D. J., Gallavardin, S., Froyd, K. D., Johnston, M. V., Middlebrook, A. M., Reinard, M. S., Thomson, D. S., Thornberry, T., and Wexler, A. S.: Distribution of lead in single atmospheric particles, Atmospheric Chemistry and Physics, 7, 3195-3210, 2007.

Murray, B. J., Wilson, T. W., Dobbie, S., Cui, Z., Al-Jumur, S. M. R. K., Möhler, O., Schnaiter, M., Wagner, R., Benz, S., Niemand, M., Saathoff, H., Ebert, V., Wagner, S., and Kärcher, B.: Heterogeneous nucleation of ice particles on glassy aerosols under cirrus conditions, Nature Geoscience, 3, 233-237, 2010.

Pratt, K. A., Heymsfield, A. J., Twohy, C. H., Murphy, S. M., DeMott, P. J., Hudson, J. G., Subramanian, R., Wang, Z., Seinfeld, J. H., and Prather, K. A.: In Situ Chemical Characterization of Aged Biomass-Burning Aerosols Impacting Cold Wave Clouds, Journal of the Atmospheric Sciences, 67, 2451-2468, 2010.

Pratt, K. A., and Prather, K. A.: Aircraft measurements of vertical profiles of aerosol mixing states, Journal of Geophysical Research-Atmospheres, 115, D11305, 2010.

Pratt, K. A., Murphy, S. M., Subramanian, R., DeMott, P. J., Kok, G. L., Campos, T., Rogers, D. C., Prenni, A. J., Heymsfield, A. J., Seinfeld, J. H., and Prather, K. A.: Flight-based chemical characterization of biomass burning aerosols within two prescribed burn smoke plumes, Atmospheric Chemistry and Physics, 11, 12549-12565, 2011.

Prenni, A. J., DeMott, P. J., Sullivan, A. P., Sullivan, R. C., Kreidenweis, S. M., and Rogers, D. C.: Biomass burning as a potential source for atmospheric ice nuclei: Western wildfires and prescribed burns, Geophysical Research Letters, 39, n/a-n/a, 2012.

Rebotier, T. P., and Prather, K. A.: Aerosol time-of-flight mass spectrometry data analysis: a benchmark of clustering algorithms, Analytica chimica acta, 585, 38-54, 10.1016/j.aca.2006.12.009, 2007.

Rogers, D. C., DeMott, P. J., Kreidenweis, S. M., and Chen, Y. L.: Measurements of ice nucleating aerosols during SUCCESS, Geophysical Research Letters, 25, 1383-1386, 1998.

Rolph, G. D.: Real-time Environmental Applications and Display sYstem (READY) Website (http://ready.art.noaa.gov), NOAA Air Resources Laboratory, Silver Spring MD, 2015.

Roth, A.: Untersuchungen von Aerosolpartikeln und Wolkenresidualpartikeln mittels Einzelpartikel-Massenspektrometrie und optischen Methoden, PhD thesis, University of Mainz, Germany, urn:nbn:de:hebis:77-37770, 2014.

Roth, A., Schneider, J., Klimach, T., Mertes, S., van Pinxteren, D., Herrmann, H., and Borrmann, S.: Aerosol properties, source identification, and cloud processing in orographic clouds measured by single particle mass spectrometry on a Central European mountain site during HCCT-2010, Atmospheric Chemistry and Physics 15, 24419-24472, 2016.

Saathoff, H., Moehler, O., Schurath, U., Kamm, S., Dippel, B., and Mihelcic, D.: The AIDA soot aerosol characterisation campaign 1999, Journal of Aerosol Science, 34, 1277-1296, 2003.

Sullivan, R. C., Petters, M. D., DeMott, P. J., Kreidenweis, S. M., Wex, H., Niedermeier, D., Hartmann, S., Clauss, T., Stratmann, F., Reitz, P., Schneider, J., and Sierau, B.: Irreversible loss of ice nucleation active sites in mineral dust particles caused by sulphuric acid condensation, Atmospheric Chemistry and Physics, 10, 11471-11487, 2010.

Tenberken-Pötzsch, B., Schwikowski, M., and Gäggeler, H. W.: A method to sample and separate ice crystals and supercooled cloud droplets in mixed phased clouds for subsequent chemical analysis, Atmospheric Environment, 34, 3629-3633, 2000.

Tobo, Y., DeMott, P. J., Hill, T. C. J., Prenni, A. J., Swoboda-Colberg, N. G., Franc, G. D., and Kreidenweis, S. M.: Organic matter matters for ice nuclei of agricultural soil origin, Atmospheric Chemistry and Physics, 14, 8521-8531, 2014.

Twohy, C. H., and Poellot, M. R.: Chemical characteristics of ice residual nuclei in anvil cirrus clouds: evidence for homogeneous and heterogeneous ice formation, Atmospheric Chemistry and Physics, 5, 2289-2297, 2005.

Twohy, C. H., DeMott, P. J., Pratt, K. A., Subramanian, R., Kok, G. L., Murphy, S. M., Lersch, T., Heymsfield, A. J., Wang, Z., Prather, K. A., and Seinfeld, J. H.: Relationships of Biomass-Burning Aerosols to Ice in Orographic Wave Clouds, Journal of the Atmospheric Sciences, 67, 2437-2450, 2010.

von der Weiden, S.-L., Drewnick, F., and Borrmann, S.: Particle Loss Calculator - a new software tool for the assessment of the performance of aerosol inlet systems, Atmospheric Measurement Techniques, 2, 479-494, 2009.

Weingartner, E., Nyeki, S., and Baltensperger, U.: Seasonal and diurnal variation of aerosol size distributions (10<D<750 nm) at a high-alpine site (Jungfraujoch 3580 m asl), Journal of Geophysical Research-Atmospheres, 104, 26809-26820, 1999.

Wilson, T. W., Ladino, L. A., Alpert, P. A., Breckels, M. N., Brooks, I. M., Browse, J., Burrows, S. M., Carslaw, K. S., Huffman, J. A., Judd, C., Kilthau, W. P., Mason, R. H., McFiggans, G., Miller, L. A., Najera, J. J.,

Polishchuk, E., Rae, S., Schiller, C. L., Si, M., Temprado, J. V., Whale, T. F., Wong, J. P., Wurl, O., Yakobi-Hancock, J. D., Abbatt, J. P., Aller, J. Y., Bertram, A. K., Knopf, D. A., and Murray, B. J.: A marine biogenic source of atmospheric ice-nucleating particles, Nature, 525, 234-238, 2015.

Wise, M. E., Baustian, K. J., Koop, T., Freedman, M. A., Jensen, E. J., and Tolbert, M. A.: Depositional ice nucleation onto crystalline hydrated NaCl particles: a new mechanism for ice formation in the troposphere, Atmospheric Chemistry and Physics, 12, 1121-1134, 2012.

Worringen, A., Kandler, K., Benker, N., Dirsch, T., Mertes, S., Schenk, L., Kästner, U., Frank, F., Nillius, B., Bundke, U., Rose, D., Curtius, J., Kupiszewski, P., Weingartner, E., Vochezer, P., Schneider, J., Schmidt, S., Weinbruch, S., and Ebert, M.: Single-particle characterization of ice-nucleating particles and ice particle residuals sampled by three different techniques, Atmospheric Chemistry and Physics, 15, 4161-4178, 2015.

Zhang, Q., Jimenez, J. L., Canagaratna, M. R., Allan, J. D., Coe, H., Ulbrich, I., Alfarra, M. R., Takami, A., Middlebrook, A. M., Sun, Y. L., Dzepina, K., Dunlea, E., Docherty, K., DeCarlo, P. F., Salcedo, D., Onasch, T., Jayne, J. T., Miyoshi, T., Shimono, A., Hatakeyama, S., Takegawa, N., Kondo, Y., Schneider, J., Drewnick, F., Borrmann, S., Weimer, S., Demerjian, K., Williams, P., Bower, K., Bahreini, R., Cottrell, L., Griffin, R. J., Rautiainen, J., Sun, J. Y., Zhang, Y. M., and Worsnop, D. R.: Ubiquity and dominance of oxygenated species in organic aerosols in anthropogenically-influenced Northern Hemisphere midlatitudes, Geophysical Research Letters, 34, L13801, 2007.

Atmos. Chem. Phys. Discuss., doi:10.5194/acp-2016-365, 2016
Manuscript under review for journal Atmos. Chem. Phys.
Published: 9 June 2016

Atmospheric Chemistry and Physics Discussions

Table 1: Clustering parameter applied in the data evaluation. (For details and the meaning of the parameters see Roth, 2014)

Preprocessing type	Power each mz
Preprocessing power	0.5
Normalization type	Sum
Initialization type	Find different start cluster
Cluster difference	0.7
Distance	Correlation
Fuzzifier	1.2
Fuzzy abort	0.0001

Atmos. Chem. Phys. Discuss., doi:10.5194/acp-2016-365, 2016
Manuscript under review for journal Atmos. Chem. Phys.
Published: 9 June 2016

Atmospheric Chemistry and Physics Discussions

Table 2: Investigated particles types with the corresponding generation procedure, manufacturer and purity where applicable data.

Particle type	Generation procedure	Manufacturer
Bacteria	AIDA (suspension)	
Grounded leaves	AIDA (mechanically dispersed)	
Pollen	AIDA/washing-water	
Cellulose	Mechanically dispersed	Sigma Aldrich
Sea salt	Suspension/solution	Sigma Aldrich
Biomass burning	Combustion (chimney)	
Brown coal	Combustion (chimney)	
Cigarette smoke	Combustion (closed room)	
Cooking/barbecue emissions	Directly sampled during a Barbecue (courtyard)	
Fuel exhaust	Directly sampled at the exhaust pipe	
PAH	Suspension	Fluka (level of purity ≥ 98 %) SUPLECO Analytical (99.9 % purity)
Soot	AIDA (combustion)	
Mineral	AIDA (suspension)	
Desert dust	AIDA (suspension)	
Soil dust	AIDA (suspension)	
Volcano dust	AIDA (suspension)	
Additional investigated biological particles		
Alanine	suspension	Roth (purity ≥ 99 %)
Cysteine	suspension	Sigma Aldrich (purity 97 %)
Glutamic acid	suspension	Alfa Aesar (purity 99 %)
Leucine	suspension	Fluka (purity > 99 %)
Proline	suspension	Roth (purity ≥ 98.5 %)
Tryptophan	suspension	Roth
Valine	suspension	Roth (purity ≥ 98.5 %)
Glucose	suspension	Roth (purity ≥ 99.5 %)
Sucrose	suspension	Roth (purity ≥ 99.5 %)
Riboflavin	suspension	Acros Organics (purity 98 %)
Chlorophyll	suspension	Roth
Hemoglobin	suspension	Sigma Aldrich

Atmos. Chem. Phys. Discuss., doi:10.5194/acp-2016-365, 2016
Manuscript under review for journal Atmos. Chem. Phys.
Published: 9 June 2016

Table 3: Overview of the different measured particle classes from primary biological, sea salt, combustion and mineral sources with their specific marker peaks, and the number of spectra which include these marker peaks. The uncertainty, as also provided, is calculated from number of spectra which include the marker peaks divided by the whole number of spectra measured of the particular particle type. The peaks marked in red are the specific marker peaks of each particle class and the peaks marked in blue show the typical marker peaks of one type. – designates the anion spectra and + the cation spectra.

Particle class	Particle type	Marker peaks [m/z]	Number of mass spectra with marker peaks	Comments
primary biological	Bacteria	-: 16, 26, 42, **45**, **63**, **71**, **79**, 96, 97 +: **23**, 39, **47**, 56, **97**	1042 (42 %)	Snomax® shows no Peak at m/z +56, 97
	Grounded maple leaves	-: 62, 97, **125**, **195** +: C_n: 12-36, **18**, 27, **30**, 39, **58**	93 (48 %)	
	Pollen	-: 26, 42, **45**, **59**, 63, **71**, **79**, 97 +: 15, 23, 39, **40**, **47**, **58**, **59**	1277 (61 %)	Birch pollen shows additionally peaks at m/z -63, 23, 56
	Cellulose	-: C_n: 24-48, **26**, 42, 62 +: C_n: 12-36, 27, **40**, **56**, **113**, **115**	196 (18 %)	Microcrystalline cellulose shows different fragmentation pattern: m/z – 71, **-125**, **-195**, **18**, **30**, **58** (106 spectra of 454 (23 %))
sea salt	Sea salt	-: 24, 45, 60, **95**, 96, 97, **99**, 135, 158 +: **23**, 24, 39, 40, **46**, **81**, **83**, 97, **139**	173 (84 %)	
combustion	Biomass burning	-: **C_n: 24-144**, **26**, 79, 97 +: **C_n: 12-192**, **23**, **39**	7436 (29 %)	
	Brown coal	-: **C_n: 24-132**, 26, **80**, 97 +: **C_n: 12-132**, **23**, **39**	53 (54 %)	
	Cigarette smoke	**-:** 26, 42, 46 +: **C_n: 12-36**, 27, 39, **50**, **51**, **63**, **77**, **115**	13017 (35 %)	Measurements after smoke inhalation show no PAH-fragmentation
	Cooking/barbecue emissions	-: 26, 42, 46, 97 +: 23, 39, **46**, **81**, **83**, **97**, **113**	299 (60 %)	
	Fuel exhaust	-: **C_n: 24-60**, 26, 46, 62, 79, **80**, 97 +: **C_n: 12-60**, 23, 27, 39, **40**	470 (40 %)	Incomplete combustions having weaker C_n-fragmentation and no peak at m/z -80
	PAH	-: 26, 79, 97 +: 27, **50/51**, **63**, **77**, **91**	419 (37 %)	
	Soot	-: **C_n: 12-156**, 26 +: **C_n: 12-144**	190 (41 %)	
mineral	Minerals	-: C_n: 24-48 +: **C_n: 12-36**, **27**, **40**, 48, 50, **56**	827 (22 %)	
	Desert dust	-: C_n: 24-48, 26, 42, **59**, **60**, **76** +: **C_n: 12-36**, 7, **27**, **40**, 48, 54, **56**, 64	60 (20 %)	
	Soil dust	-: 26, 42, **59**, **60**, 63, **76**, **79** +: 7, **27**, 48, 54, **56**, 64	721 (33 %)	Soil dust from Switzerland „Bächli“ exhibits different fragmentation pattern in the anion spectra; cation spectra show additionally m/z 18, 30, 58 and only m/z 27 and 56 of the indicated marker peaks (891 of 2122 spectra (42 %))
	Volcano dust	-: 24, 36, 97 +: **C_n: 12-36**, 23, **27**, 28, 39, **40**, **56**	32 (37 %)	

Atmos. Chem. Phys. Discuss., doi:10.5194/acp-2016-365, 2016
Manuscript under review for journal Atmos. Chem. Phys.
Published: 9 June 2016

Atmospheric Chemistry and Physics Discussions

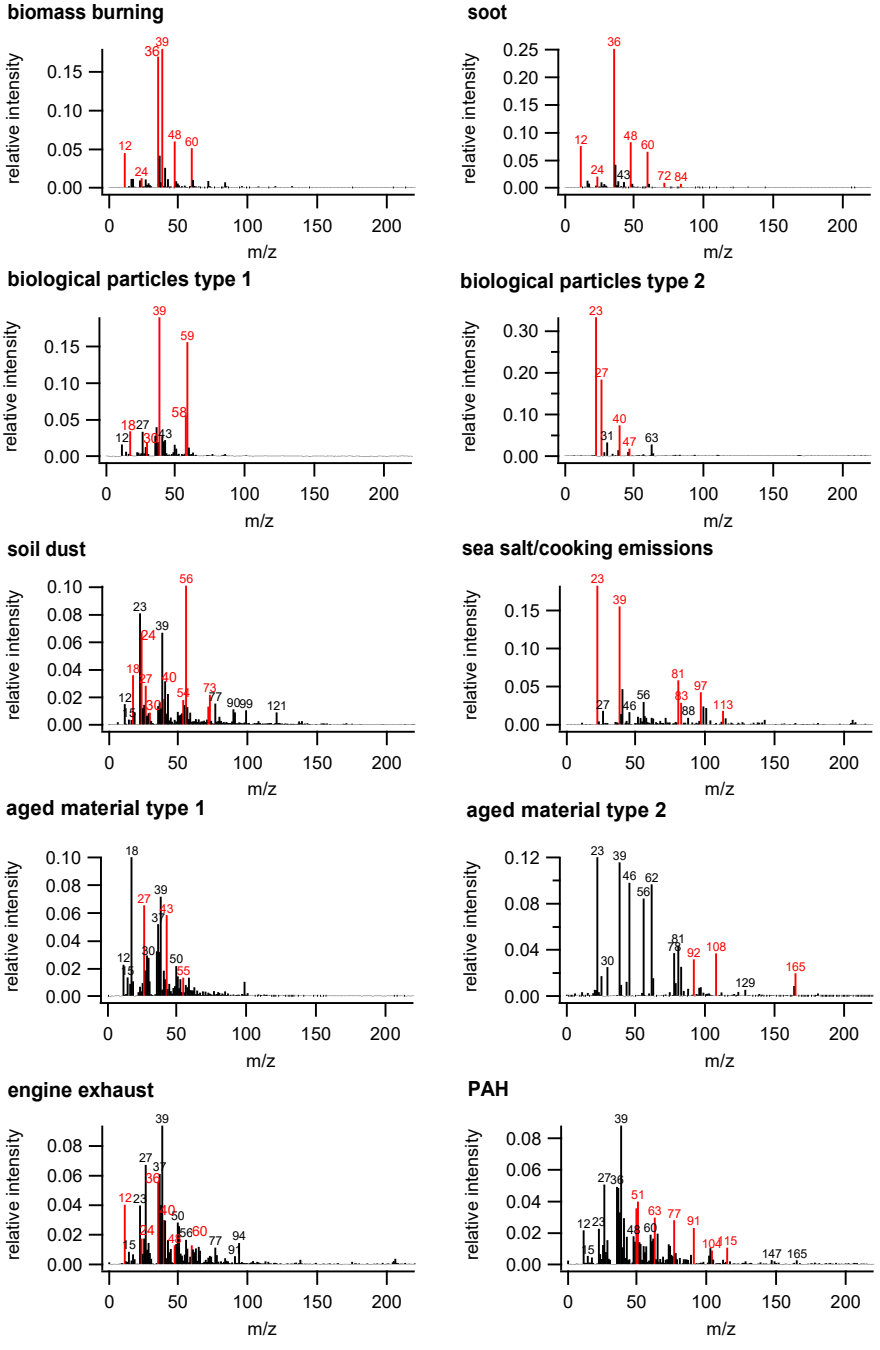

Atmos. Chem. Phys. Discuss., doi:10.5194/acp-2016-365, 2016
Manuscript under review for journal Atmos. Chem. Phys.
Published: 9 June 2016

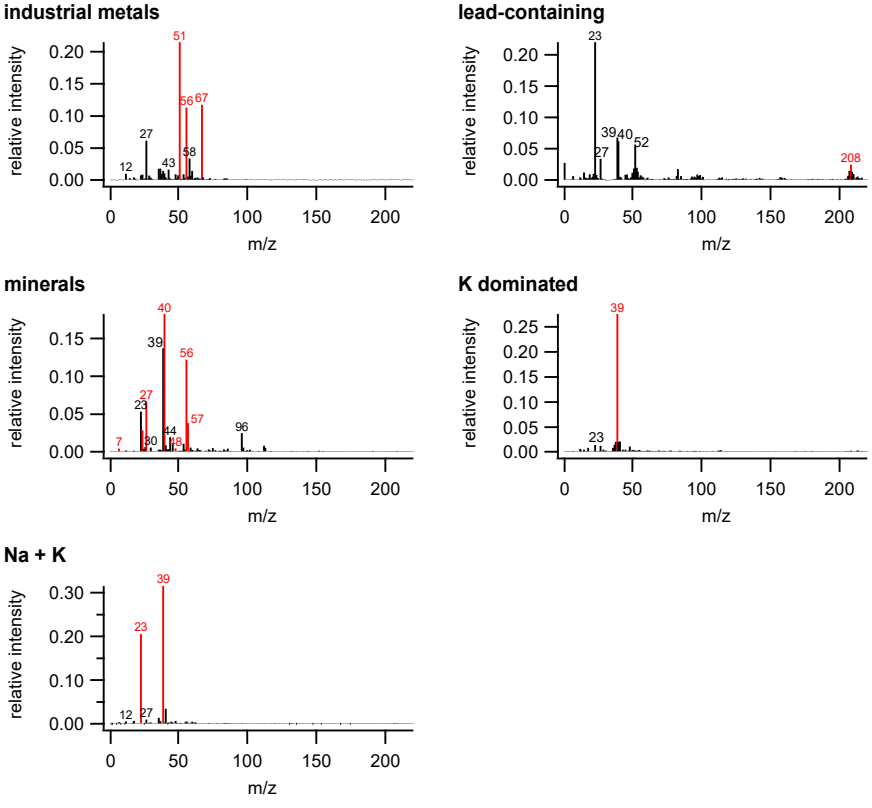

Figure 1: Average spectra (only cations) of all identified particles types from the JFJ-measurements. The classification was done according to the results from the laboratory studies (Table 3). The red highlighted peaks indicate the marker peaks used for identification of the particle type.

Atmos. Chem. Phys. Discuss., doi:10.5194/acp-2016-365, 2016
Manuscript under review for journal Atmos. Chem. Phys.
Published: 9 June 2016

Atmospheric Chemistry and Physics Discussions

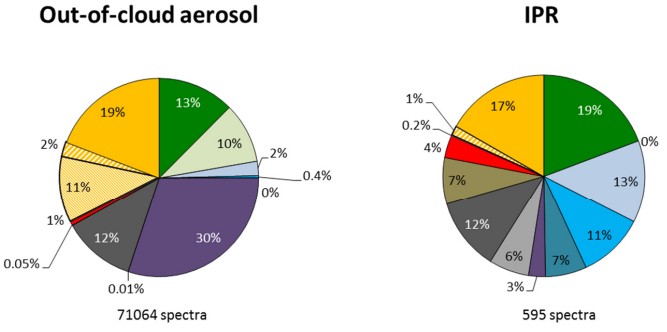

Particle type	Out-of-cloud	IPR
biological particles	8871 [13%]	114 [19%]
biomass burning	6959 [10%]	0
soil dust	1655 [2%]	78 [13%]
minerals	261 [< 1%]	63 [11%]
sea salt/cooking emissions	0	39 [7%]
aged material	21392 [30%]	16 [3%]
engine exhaust	8 [< 1%]	38 [6%]
PAH/soot	8423 [12%]	69 [12%]
lead-containing	36 [< 1%]	44 [7%]
industrial metals	399 [1%]	21 [4%]
K dominated	7665 [11%]	1 [< 1%]
Na + K	1756 [2%]	9 [1%]
others	13639 [19%]	99 [17%]

Figure 2: Relative abundance of identified particle types in all out-of-cloud particles (left) and all sampled IPR (right). Absolute number of particles and percentages are given.

Atmos. Chem. Phys. Discuss., doi:10.5194/acp-2016-365, 2016
Manuscript under review for journal Atmos. Chem. Phys.
Published: 9 June 2016

Atmospheric Chemistry and Physics Discussions

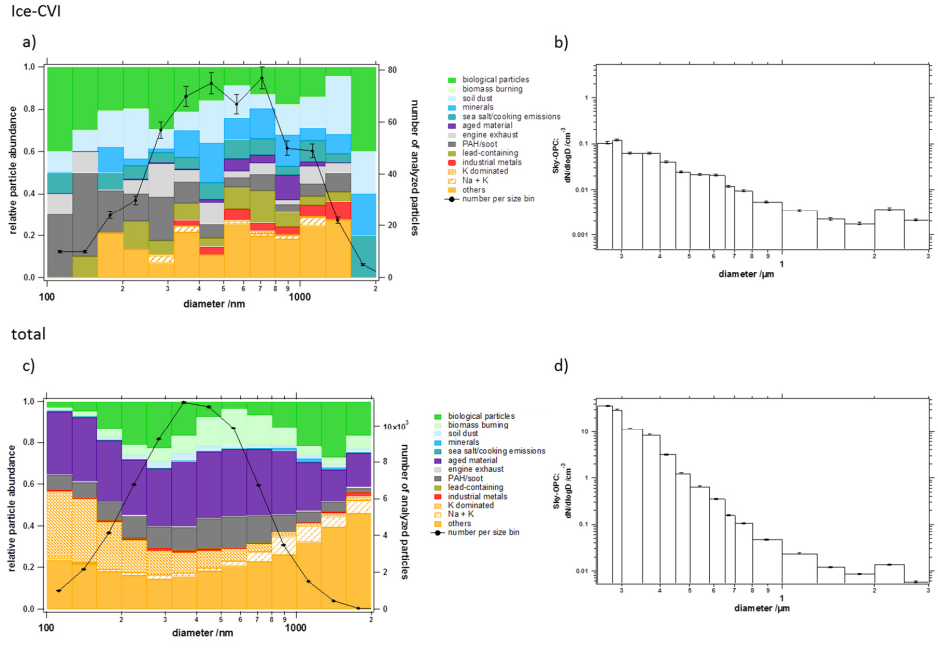

Figure 3: Size resolved composition of the IPR (a)) and out of-cloud-aerosol particles (c)) sampled with the ALABAMA and the measured size distribution of the Sky-OPC (Ice-CVI: b; total: d). The black lines in a) and c) refer to the numbers of particles per size bin (right ordinate) of which a mass spectrum was obtained by ALABAMA with error bars based on counting statistics. The errors of the Sky-OPC data results from Gaussian propagation of uncertainty, including counting statistics, the manufacturer-given error of the OPC of 3 %, and the error of the enrichment factor (4 %).

Atmos. Chem. Phys. Discuss., doi:10.5194/acp-2016-365, 2016
Manuscript under review for journal Atmos. Chem. Phys.
Published: 9 June 2016

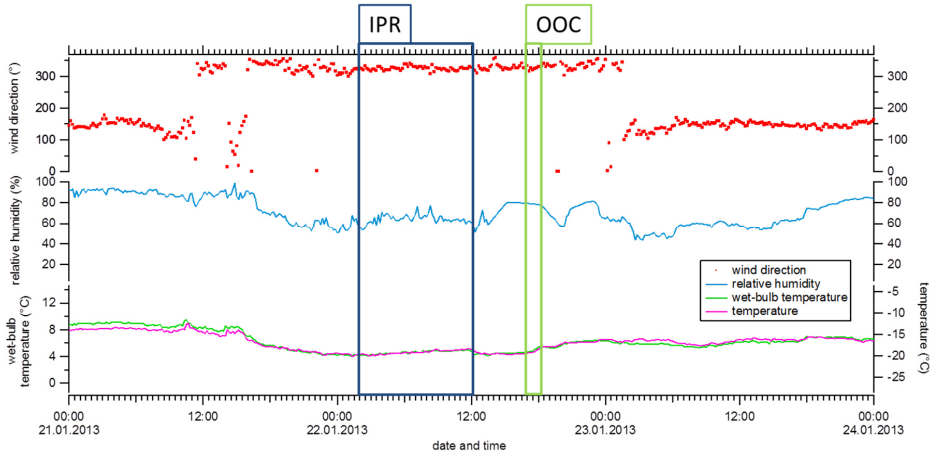

Figure 4: Wind direction, relative humidity, potential wet-bulb temperature and temperature (data from Meteo Swiss at the JFJ). The IPR sampling period is highlighted in blue, the out-of-cloud aerosol (OOC) sampling period in green.

Atmos. Chem. Phys. Discuss., doi:10.5194/acp-2016-365, 2016
Manuscript under review for journal Atmos. Chem. Phys.
Published: 9 June 2016

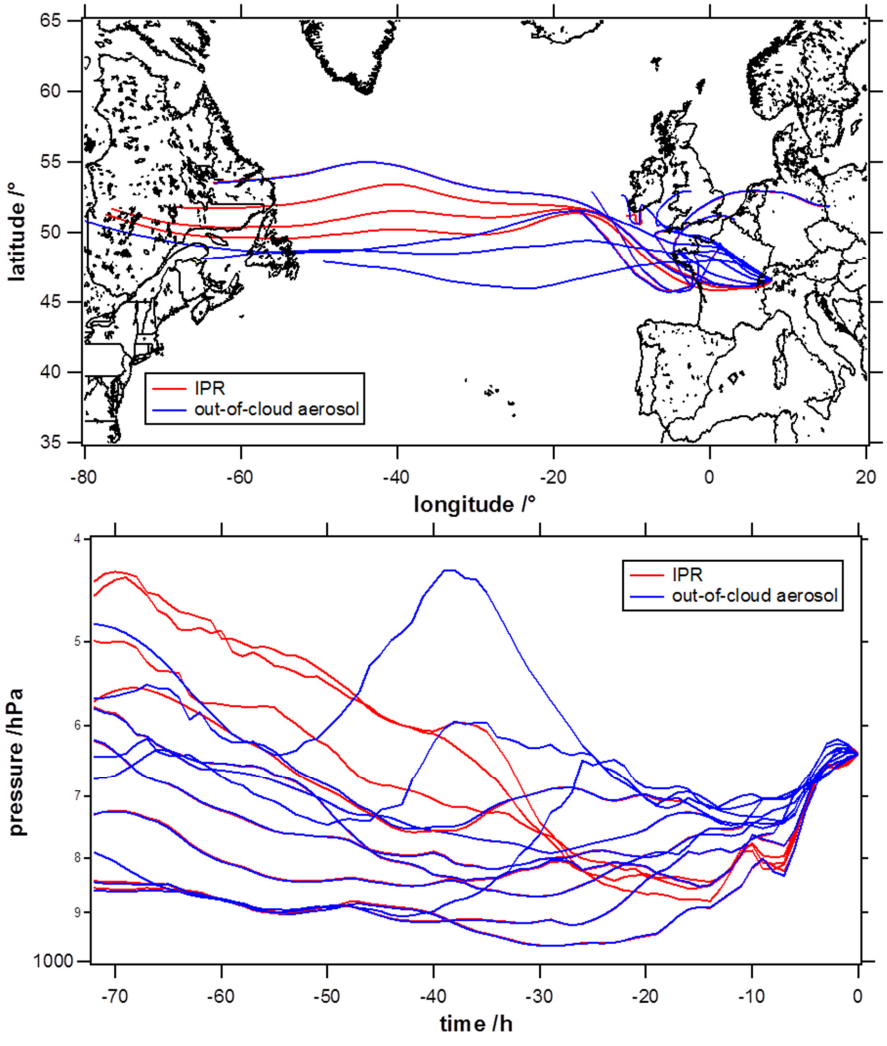

Figure 5: Back trajectories (above) and air mass pressure as a function of time (below) for both sampling periods (red: IPR; blue: out-of-cloud aerosol).

Atmos. Chem. Phys. Discuss., doi:10.5194/acp-2016-365, 2016
Manuscript under review for journal Atmos. Chem. Phys.
Published: 9 June 2016

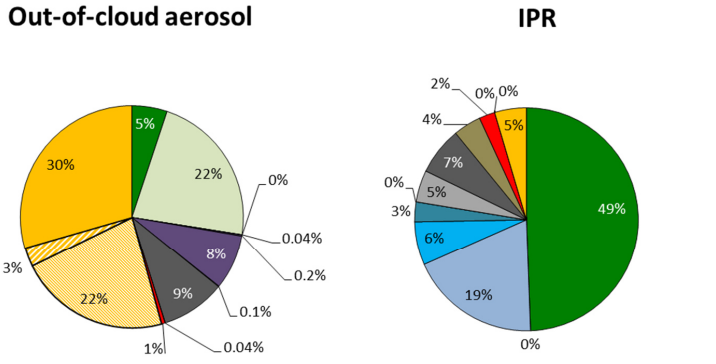

Particle type	Out-of-cloud	IPR
biological particles	469 [5%]	86 [49%]
biomass burning	2047 [22%]	0
soil dust	0	33 [19%]
minerals	4 [< 1%]	11 [6%]
sea salt/cooking emissions	16 [< 1%]	5 [3%]
aged material	735 [8%]	0
engine exhaust	10 [< 1%]	8 [5%]
PAH/soot	853 [9%]	12 [7%]
lead-containing	4 [< 1%]	7 [4%]
industrial metals	50 [1%]	4 [2%]
K dominated	2016 [22%]	0
Na + K	254 [3%]	0
others	2698 [30%]	8 [5%]

Figure 6: Comparison of the chemical composition at similar sampling conditions during each sampling period of the out-of-cloud aerosol (left) and the IPR (right).